ACS APPLIED MATERIALS & INTERFACES

Research Article

Cite This: ACS Appl. Mater. Interfaces 2018, 10, 44678−44685

www.acsami.org

Wireless Real-Time Temperature Monitoring of Blood Packages: Silver Nanowire-Embedded Flexible Temperature Sensors

Doo-Young Youn,[†,¶] Uihyun Jung,[§,¶] Muhammad Naqi,[§,¶] Seon-Jin Choi,[∥,¶] Min-Goo Lee,[⊥] Sungho Lee,[⊥] Hi-Joon Park,[#] Il-Doo Kim,*[,†,‡] and Sunkook Kim*[,§]

[†]Department of Materials Science and Engineering, Korea Advanced Institute of Science and Technology (KAIST), 291 Daehak-ro, Yuseong-gu, Daejeon 34141, Republic of Korea

[‡]Advanced Nanosensor Research Center, KAIST Institute for the NanoCentury, KAIST, Daejeon 34141, Republic of Korea

[§]Multi-Functional Nano Bio Electronics Lab, Department of Advanced Materials Science and Engineering, Sungkyunkwan University, Gyeonggi 16419, Republic of Korea

[∥]Department of Chemistry, Massachusetts Institute of Technology, 77 Massachusetts Avenue, Cambridge, Massachusetts 02139, United States

[⊥]Convergence System R&D Division, Korea Electronics Technology Institute, Gyeonggi 13509, Republic of Korea

[#]Acupuncture & Meridian Science Research Center, College of Korean Medicine, Kyung Hee University, 26, Kyungheedae-ro, Dongdaemoon-gu, Seoul 02447, Republic of Korea

Supporting Information

ABSTRACT: Real-time temperature monitoring of individual blood packages capable of wireless data transmission to ensure the safety of blood samples and minimize wastes has become a critical issue in recent years. In this work, we propose flexible temperature sensors using silver nanowires (NWs) and a flexible colorless polyimide (CPI) film integrated with a wireless data transmission circuit. The unique design of the temperature sensors was achieved by patterning Ag NWs using a three-dimensional printed mold and embedding the patterned Ag NWs in the CPI film (p-Ag NWs/CPI), which resulted in a flexible temperature sensor with electrical, mechanical, and temperature stability for applications in blood temperature monitoring. Indeed, a reliable resistance change of the p-Ag NWs/CPI was observed in the temperature range of −20 to 20 °C with a robust bending stability of up to 5000 cycles at 5 mm bending radius. Real-time and wireless temperature monitoring using the p-Ag NWs/CPI was demonstrated with the packages of rat blood. The result revealed that the stable and consistent temperature monitoring of individual blood packages could be achieved in a blood box, which was mainly attributed to the conformal attachment of the p-Ag NWs/CPI to different packages in a blood container.

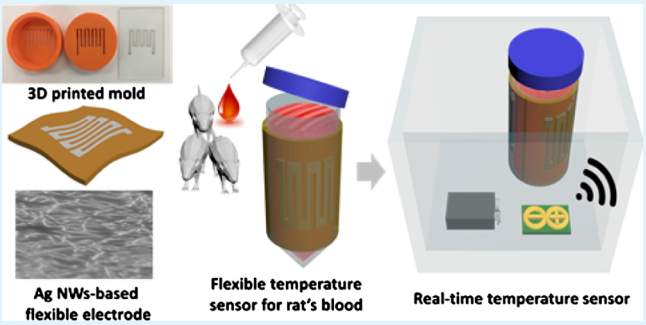

KEYWORDS: *silver nanowire, temperature sensor, 3D printer, blood temperature, flexible sensor*

1. INTRODUCTION

In recent years, new types of mobile healthcare systems have been developed by the advancements in flexible and wearable electronics including physical sensors,[1,2] chemical sensors,[3] breath analyzers,[4] and triboelectric generator.[5] In particular, physical states of objects can be monitored in real-time by combining sensors with the Internet of Things technology to transmit data to a mobile phone. Also, monitoring the long-term stability of objects is possible by measuring physical parameters over extended timescales to evaluate the transitions of states.[6,7]

Blood plays a vital role in delivering oxygen and supplying oxygen to cells of organs in the human body. It has been reported that the loss of 40% of blood can result in fatal damage to human organs and even cause death.[8] For this reason, the storage of blood packs is critical when a situation that requires emergency transfusions arise. However, when blood packs are stored under inappropriate conditions, significant metabolic changes occur, such as decreased pH, reduced adenosine 5′-triphosphate concentration, and extracellular potassium accumulation,[9,10] which result in the disposal of blood. The temperature of blood packs is particularly important for maintaining adequate conditions for red blood cells (RBCs) and the packs must not exceed 30 min at room temperature.[11] For the storage of blood, the temperature should be maintained in the range of 1−6 °C for up to 42 days,

Received: July 16, 2018
Accepted: November 29, 2018
Published: November 29, 2018

DOI: 10.1021/acsami.8b11928
ACS Appl. Mater. Interfaces 2018, 10, 44678−44685

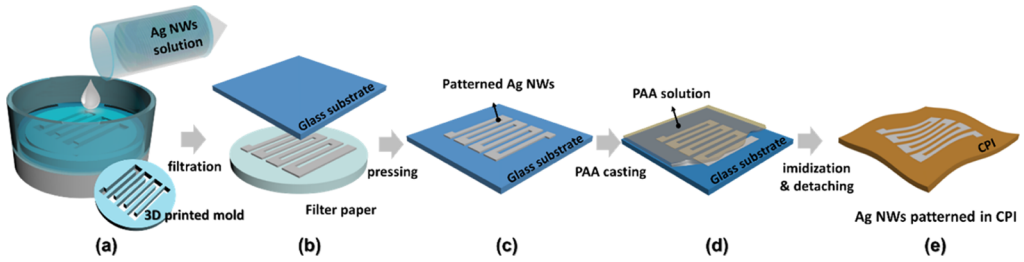

Figure 1. Schematic illustration of the fabrication process for flexible Ag NWs-patterned CPI (p-Ag NWs/CPI). (a) Filtration method. (b) Transferring of p-Ag NWs. (c) p-Ag NWs on a glass. (d) Casting of the PAA solution. (e) Imidization and detachment process.

following collection.[12−14] However, a lack of temperature data results in difficulties in understanding the progression of RBC's conditions, particularly during transportation and storage; thus, it is essential to develop a reliable and convenient sensing system to monitor the temperature of blood packs. Therefore, the systematic management of blood packs is required by monitoring the temperature of individual packages in real-time and over an extended time scale by transmitting the measured data to a mobile device via wireless communication technology.

Conventionally, measuring refrigeration temperature has been a general strategy for monitoring multiple blood packages in a chamber instead of monitoring individual packages.[15] For this reason, the conventional temperature measurement system is not suitable for blood monitoring, and it is therefore, difficult to manage the temperature of individual packages. To monitor the temperature of individual packages, a new type of temperature sensor should be developed with high flexibility and deformability. Specifically, the temperature sensor is required to be conformably attached to a curved or bent package to precisely monitor its temperature. Thus far, several types of flexible temperature sensors have been developed using diverse conductive elements on flexible substrates, including thin-metal films,[16−18] graphene film layers,[19,20] and carbon nanotubes[21,22] with high mechanical stability, which show potential for applications in flexible thermometers. Herein, carbon materials are compatible to be applied in flexible devices because of their inherent flexibility. Several studies report that graphene nanowall[23] and polyaniline fiber[24] having a high temperature coefficient of resistance (TCR) value have recently been developed as a temperature sensor but because they exhibit poor linearity over a wide temperature range, they are not suitable for use as resistance temperature detectors (RTDs). Therefore, materials for measuring the temperature using the RTD method have been mainly attempted using metallic conductors. Especially, Platinium(Pt) having chemical stability, acceptable resistivity (1.6×10^{-8} Ω m), linearity, and TCR (0.0039/°C at 20 °C) has been widely used as a typical material for RTD. However, because of its higher price and scarcity, alternative materials are highly demanding in fields such as temperature sensors.

Silver (Ag) has a TCR value (0.0038/°C at 20 °C) similar to that of Pt and has a relatively high abundance and a low price. In particular, silver nanowires (Ag NWs) have been intensively studied because they are not only mass-produced by the solution-based synthesis method but also exhibit excellent electrical properties compared to other conducting materials. Kojda et al.[25] investigated thermoelectric properties of single crystalline Ag NWs. Wang et al.[26] studied the temperature dependency of electrical properties of a single Ag NW and revealed that the NW structure exhibits higher sensitivity to changes in temperature than bulk silver, which was mainly attributed to a phonon−electron scattering effect. Although fundamental studies have shown a potential application in the field of RTDs, the chemical instability owing to the nanoscale diameter,[27] poor adhesion properties with a substrate, and unsuitable resistance values of pure Ag NWs are the significant obstacles toward their application in temperature sensors. To overcome the above problems, several researchers have carried out embedding processes to bury NWs into polymer matrices, such as poly(dimethylsiloxane),[28] polyimide,[29,30] NOA63,[31] and GFR hybrimer.[32] However, to the best of our knowledge, an Ag NW-based thermometer has not been developed yet for a real-time temperature sensing application, particularly for monitoring individual blood packages.

In this work, we developed a wireless temperature sensor using Ag NWs with high thermal sensitivity and stability for application in the real-time and long-term temperature monitoring of blood packages. Ag NWs were patterned by using a three-dimensional (3D) printed mold, which is proposed for the first time, and embedded in a colorless polyimide (CPI) film to maintain the desirable overall resistance, an acceptable sensitivity toward temperature changes, and excellent mechanical stability. The proposed flexible temperature sensor exhibits distinct linearity, reliability at various pattern lengths ranging from 25 to 152 mm in the temperature range from −20 to 20 °C, and acceptable TCR values (0.0028−0.0033/°C). As a potential application in the real-time monitoring of blood package, Ag NW-based flexible temperature sensors with the corresponding electric circuit were attached to multiple blood packages containing the blood of rat to transmit temperature data of individual packages to a mobile device via wireless communication. The proposed flexible sensor is enthusiastically designed to monitor the temperature of clinical and commercial products that can be conformally laminated on a curved and wrinkled surface.

2. RESULTS AND DISCUSSION

Figure 1 shows the fabrication procedures of flexible Ag NW-embedded CPI films. In our previous work, a highly stable and flexible conductive film has been demonstrated using Ag NWs by embedding in the CPI film.[29,33,34] In the present study, a unique patterning technique of Ag NWs was proposed using a 3D printed mold and subsequently embedded in the CPI film, which is essential to obtain linearity of the resistance with respect to temperature changes. The Ag NWs were prepared by the polyol method and the solution was dispersed in ethanol. To pattern the Ag NWs electrode, a straight-winding mold structure with an open space of 2.0 mm was fabricated using a 3D printer. Patterning of Ag NWs on a filter paper was performed by a filtration process, in which the Ag NW-

DOI: 10.1021/acsami.8b11928
ACS Appl. Mater. Interfaces 2018, 10, 44678−44685

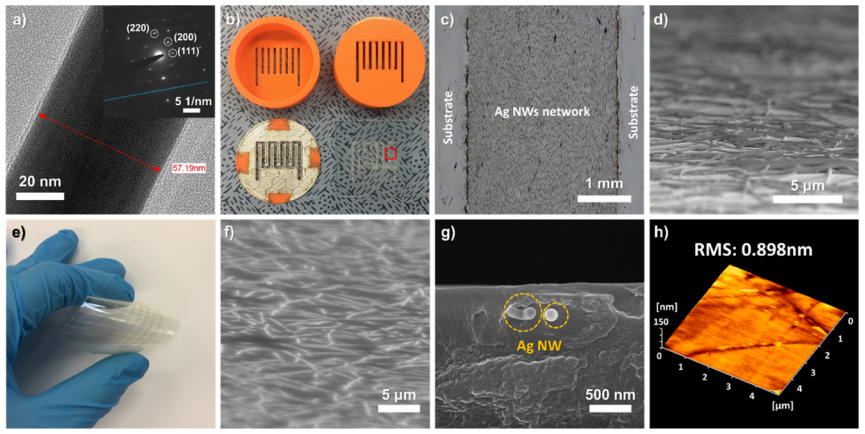

Figure 2. (a) TEM image of an Ag NW and its SAED pattern (shown as the inset). (b) Photographs of 3D-printed molds and Ag NW electrode patterned by the mold (right-bottom). (c) Enlarged OM image of the selected area (red box in b) of the p-Ag NWs electrode on a glass substrate. (d) SEM image of the p-Ag NWs electrode on a glass substrate. (e) Photograph of Ag NWs/CPI electrode bent by fingers. (f) Tilted-view and (g) cross-sectional SEM image of the p-Ag NWs/CPI electrode. (h) AFM image of the p-Ag NWs/CPI electrode.

dispersed solution was vacuum filtrated using the interdigitated 3D mold on the filter paper (Figure 1a). A subsequent Ag NW transfer process from the filter paper to a glass substrate was carried out using a pneumatic press equipment (Figure 1b). After the transfer process, the patterned Ag NW electrode remained on the glass substrate without any deformation (Figure 1c). In order to embed the patterned electrode into the CPI film, a precursor solution of polyamic acid (PAA) was printed on the patterned Ag NWs glass substrate using a doctor blade (Figure 1d). Finally, an Ag NWs-embedded and freestanding CPI film was achieved after the imidization process by heat treatment and a subsequent detachment process (Figure 1e).

Figures 2a and S1 show the transmission electron microscopy (TEM) image of an Ag NW with a diameter of about 50 nm from a minimum value of 37.13 nm to a maximum value of 61.36 nm. The selected area electron diffraction (SAED) pattern revealed the crystallinity of the five-fold twinned pentagonal structure.[35] From the clear spots of (111), (200), and (220) facets, it can be confirmed that the Ag NW exhibits high crystallinity. Also, the parallel spots along the blue line of inset can be interpreted as a double-diffraction effect because of the superposition of subcrystals.[36] Generally, Ag NW-based electrodes exhibit a relatively low sheet resistance (~5−50 Ω/sq) when networks are formed among Ag NWs. In order to use Ag NWs for the temperature sensor, an appropriate resistance level of the electrode is critical. If the resistance of an Ag NW electrode is too low, an electrical signal/noise discrimination becomes difficult to distinguish. Lowering the density of the Ag NW network is problematic because of unstable electrical contacts.

For this reason, the patterned Ag NW structure is a promising solution to increase the resistance of the electrode by increasing the electrical pathway. We have controlled the resistance of the Ag NW network based on the equation for the resistance of a general conductor: $R = \rho(L/A)$, where L is the length of the conductor, A is the cross-sectional area of the conductor, and ρ is the electrical resistivity. As shown in the equation, the resistance is proportional to the value of L. Thus, the resistance can be effectively increased without changing the density of the Ag NW electrode. To elongate the electrical pathway combined with conventional vacuum filtering technique, we used a 3D-printed mold as a pattern mask for the selected filtration of Ag NWs on a glass substrate. Figure 2b shows the 3D molds with top, bottom, a cross-sectional structure, and patterned Ag NWs (hereafter, p-Ag NWs) using the 3D mold on a glass substrate, respectively. After the filtration process, the Ag NWs were patterned on a glass substrate with the same pattern as the open space on the 3D mold structure. To observe the microstructure of the electrode, the p-Ag NWs electrode was analyzed using an optical microscope (Figure 2c, red box in 2b). Ag NWs were uniformly dispersed and patterned along the line, whereas Ag NWs were not observed in the area blocked by the 3D mold. To further understand the microstructural characterization of Ag NW-based electrodes, scanning electron microscope (SEM) and atomic force microscope (AFM) analyses were conducted. Figure 2d shows a tilted SEM image of the p-Ag NWs electrode on the glass substrate. Ag NWs were tangled and well-distributed. In particular, Ag NWs were extruded on the surface where multiple Ag NWs were overlapped and some of them were protruded like spines (Figure S2). Figure 2e presents a photograph of the patterned Ag NWs embedded in the CPI film (hereafter, p-Ag NWs/CPI) during bending of the film with an overall dimension of 5 cm × 5 cm. The p-Ag NWs electrode was embedded in the CPI film without changing the shape of the electrode even after the embedding process. A tilted-SEM image of p-Ag NW/CPI shows a flat surface morphology because of the fully embedded nature of Ag NWs (Figure 2f). Cross-sectional SEM observation reveals fully embedded Ag NWs in the CPI film, which can ensure the mechanical and long-term stability of Ag NW-based temperature sensors (Figure 2g). The surface roughness was substantially reduced as evidenced in the low root mean square roughness (0.90 nm) of the p-Ag NWs/CPI as compared to the roughness (26.77 nm) of p-Ag NWs on the glass substrate (Figures 2h and S3). To detect blood temperature with high accuracy, the entire surface of the sensing part of the flexible sensor must be in direct contact to the blood package. In this regard, the surface roughness is an important parameter to ensure conformal contact between p-Ag NWs/CPI and the blood package. Moreover, the low surface roughness can enhance the conformal attachment of p-Ag NWs/CPI on a curved and wrinkled surface.

Coefficient of thermal expansion (CTE) was considered to investigate whether the CPI used as the substrate could affect

DOI: 10.1021/acsami.8b11928
ACS Appl. Mater. Interfaces 2018, 10, 44678−44685

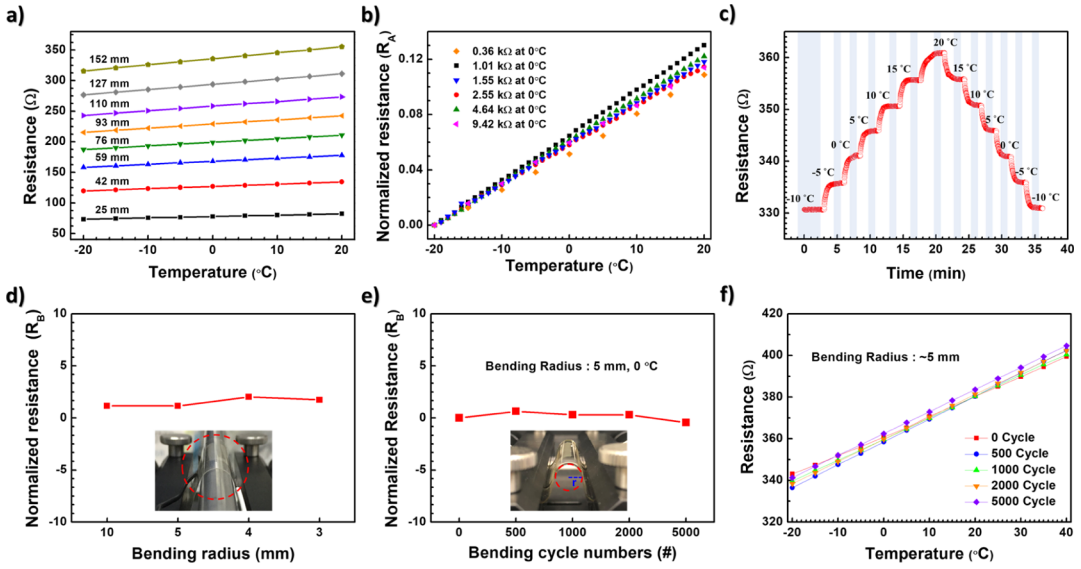

Figure 3. (a) Resistance behavior of the Ag NW temperature sensor under different temperatures concerning various lengths. (b) Normalized resistance variations according to a temperature of various p-Ag NWs/CPI temperature sensors having different resistances. (c) Hysteresis behavior of the temperature sensor response at various temperatures with a holding time interval of 1 min. (d) Resistance variation concerning the bending radius (10, 5, 4, and 3 mm) and (e) bending cycles of up to 5000 cycles. (f) Temperature vs resistance variation concerning the various bending cycles (0, 500, 1000, 2000, and 5000).

the resistance value of the electrodes. The CTEs of Ag and CPI are 18.9×10^{-6} and 46.79×10^{-6} K^{-1}, respectively.[37,38] It is about 100 times lower than the TCR value of Ag NWs, which is considered to have a minor influence on the resistance change of the sensor. Therefore, it is reasonable to insist that the thermoelectric behavior is originated from the resistance changes of Ag NWs. Figure 3 presents electrical and mechanical measurements to investigate the suitability and robustness of the p-Ag NWs/CPI as a flexible temperature sensor. To obtain reliable electrical properties, titanium/gold (Ti/Au) was deposited as an electrode via an e-beam evaporator with a thickness rate of 20 nm/100 nm, respectively. The p-Ag NWs/CPI exhibited a resistance of 360 Ω to 9.42 kΩ according to the density of Ag NW solution. Considering a resistance distribution and reliability of the sensor, a resistance of 2.0 kΩ or less is suitable for applications in flexible temperature sensors (Figure S4). The Ag NW electrode tends to reduce the resistance and the resistance variation after embedding. This phenomenon is due to the formation of junctions between the crossed Ag NWs because of the heat treatment process at 230 °C during the embedding process.[39] The temperature responses concerning the nomarlized resistance (R_A) of the Ag NW-based temperature sensor have been analyzed while considering the various lengths (25, 42, 59, 76, 93, 110, 127, and 152 mm) under the temperature range of −20 to 20 °C. (Figure 3a). Herein, R_A is expressed as $[(R_r - R_m)/R_r]$, where R_r and R_m are the measured resistance at the reference temperature (−20 °C) and at the temperature range of −20 °C to 20 °C, respectively. These results exhibit no significant changes in the TCR value (0.00311/°C approx.) at different lengths of p-Ag NWs and the resistance of the temperature sensor can be varied by changing the length of the p-Ag NWs sensor with a stable TCR value. In addition, the graphical representation of the Ag NW temperature sensor according to the various lengths ranging from 25 to 152 mm has been depicted in the Supporting Information along with the design layout of the temperature sensor (Figure S5). In addition, different p-Ag NWs sensor samples having resistances ranging from 0.36 to 9.42 kΩ at 0 °C exhibited an excellent linear response and similar TCR value (0.0028−0.0033/°C) ranging from −20 to 20 °C (Figure 3b). To reveal the thermoelectric reliability of the p-Ag NWs sensor, the hysteresis behavior was investigated at every 5 °C within the range of −10 to 20 °C for 1 min interval (Figure 3c). The result revealed that the p-Ag NWs/CPI temperature sensor exhibited reliable and reversible resistance transitions in the temperature range with fast responding time.

Mechanical stability at a high level of stress is required to monitor the temperature of wrinkled blood packages sustaining different surface shapes.[40,41] To investigate the robust tolerance and deformability of our flexible temperature sensor against mechanical stresses, static and cyclic bending tests were conducted. Figure 3d shows the deformability results of the p-Ag NWs/CPI temperature sensor regarding the normalized resistance (R_B) at various bending radii (3, 4, 5, and 10 mm) retaining an upward bending condition. Herein, R_B is expressed as the resistance ratio before and after the bending test followed by the given equation, $[R_B = (R_0 - R_b)/R_0 \times 100\ (\%)]$, where R_0 and R_b are the resistances measured before and after the bending test, respectively. The error rate (%) is examined only 2.02% at the mentioned bending radii compared to the related flat conditions. Furthermore, in order to carefully investigate mechanical deformation, repetitive cyclic bending tests were performed under 0, 500, 1000, 2000, and 5000 bending cycles at a bending radius of 5 mm using a p-Ag NWs sensor having a film thickness of about 40 μm (Figure 3e). The results indicate that the performance of the proposed flexible sensor was not significantly degraded by gradually increasing the bending cycle and the error rate was examined around 0.62%. The flexible property of the CPI film and the unique embedded structure of Ag NWs allowed our sensor to have substantial durability against mechanical stresses. Figure 3f exhibits the changes in the resistance at various bending cycles (up to 5000 cycles) with a 5 mm radius

DOI: 10.1021/acsami.8b11928
ACS Appl. Mater. Interfaces 2018, 10, 44678−44685

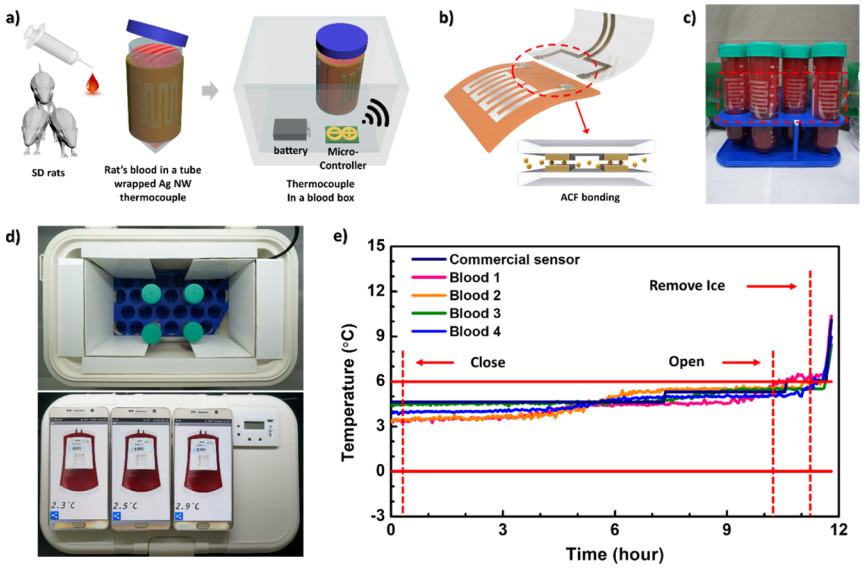

Figure 4. (a) Prototype of sensing system using the flexible p-Ag NWs/CPI. (b) Electrode bonding between the p-Ag NWs/CPI and gold wire. Optical image of (c) the sensor attached to blood tubes, (d) placing of blood tubes in the blood box (top) and real-time monitoring of blood temperature stored in the blood box (bottom). (e) Graphical representation of a temperature sensor attached to the blood tube inside the box for 12 h.

of curvature under the temperature range of −20 to 40 °C. The 0.12 Ω/°C difference is measured after the bending cycles (up to 5000 cycles) compared to before the bending test. As evidenced in stable resistance transition property as well as mechanical stability, the p-Ag NWs/CPI is highly promising for reliable and reproducible temperature monitoring under the normal storage temperature range (1−6 °C) of blood packages.

To demonstrate real-time temperature monitoring, we developed a wireless temperature monitoring system using animal blood samples (Figure 4a). Blood from Sprague Dawley rat was selected instead of human blood for legal authorization. The sensor circuitry was assembled with the following components: (1) a wheat-stone bridge resistor network (2) an Arduino (Uno) controller, (3) a bluetooth device (HC-06), and (4) a micro secure digital (SD) card module (Figure S6). To obtain the accuracy of the p-Ag NWs/CPI thermometer in a closed environment, an anisotropic conductive film (ACF) bonder was used for the perfect contact between the electrodes of the temperature sensor and the driving circuitry assembled on a customized printed circuit board (PCB) (Figure 4b). Although a blood tube has a curved and rounded shape, the p-Ag NWs/CPI thermometers were uniformly attached to the blood tubes because of a deformable structure of the thermometer (Figure 4c). The arrangement and the real-time monitoring of individual blood tubes in the customized blood box were described in the optical photograph, shown in the upper and lower side of Figure 4d, respectively. The blood box with a built-in commercial sensor can measure the internal temperature inside the box and allow for the comparison of each blood sample to the internal temperature. The comparison of the blood sample temperature to the internal temperature showed minor variations depending on the location, as demonstrated in Figure 4d (blood temperature: 2.3, 2.5, 2.9 °C, and internal temperature: 2.57 °C). In the present experiment, the temperature variations of blood samples stored in the blood box analyzed for 12 h were divided into three intervals (marked as red dotted lines), depicting (i) an appropriate range of temperature (0−6 °C) after closing the blood box, (ii) a slight fluctuation in the temperature after opening the blood box, and (iii) a sharp increase in temperature after removing the ice packs (Figure 4e). In addition, the real-time monitoring of the CPI-based Ag NW temperature sensor was also performed in the vacuum environment, with temperature ranging from 0 to 7 °C that can be visualized in Video S1. As a result, we demonstrated a unique tracking and real-time temperature monitoring system based on a flexible Ag NW temperature sensor to prevent damages caused by blood coagulation and maintain the potency of the blood.

Although there remain challenges for optimizing the structure of the thermometer, the proposed thermometer could also be applied to various types of package measurements that require flexibility and real-time monitoring, including packaging that houses temperature-sensitive products, such as human & animal specimens, vaccines, pathogens, and biological substances. Furthermore, it could be extended to a form that can attach directly to human or animal.

3. CONCLUSIONS

In summary, we present a flexible temperature sensor monitoring in real time, in which Ag NWs patterned by a 3D printed mold are embedded on the flexible CPI film to achieve appropriate overall resistance range by controlling Ag NW density and a pattern length. The proposed p-Ag NWs temperature sensors show a distinct linear and stable behavior under various temperatures ranging from −20 to 20 °C. In addition, a TCR value of 0.00311/°C with linearity was obtained regardless of the length of the patterned Ag NWs despite the difference in resistance values, but slightly different TCR values (0.0028−0.0033/°C) when the density of NW was changed. The mechanical stress and strain tests were also performed to confirm the deformability and accuracy to ensure reliable temperature sensing on various surface morphologies. The results exhibit consistent stable temperature sensing under various static and bending cycle experiments. In this work, a

DOI: 10.1021/acsami.8b11928
ACS Appl. Mater. Interfaces 2018, 10, 44678−44685

simple medical device has been designed to monitor and track the temperature transitions of blood, which enables both online (BLE) and offline (SD-card) data transmission and demonstrates the scalability of the new practical application areas of NW materials. The temperature fluctuations in the blood extracted from Sprague Dawley rat housed in a medical box were examined for 12 h under a temperature range of 0 to 6 °C. We expect that the presented system will allow long-term surveys to monitor and secure medical products and facilitate the enhancement of wearable electronics in the medical field.

4. EXPERIMENTAL SECTION

4.1. Materials. All chemicals were used without further purification and purchased from commercial sources as follows; silver nitrate ($AgNO_3$), silver chloride (AgCl), *N*,*N*-dimethylacetamide (DMAc, Sigma-Aldrich), 4,4′-(hexafluoroisoprolyidene)diphthalic anhydride (6-FDA, Sigma-Aldrich), 3,3′-diaminodiphenyl sulfone (APS), polyvinylpyrrolidone (PVP, MW 1300k and 10k, Sigma-Aldrich), ethylenediaminetetraacetic acid (EDTA) coated bottle, ethylene glycol (EG) (Sigma-Aldrich), ethanol, and acetone.

4.2. Synthesis of Ag NWs and PAA Solution. Ag NWs were synthesized using a hydrothermal method. First, 6.68 g of PVP was dissolved in EG under magnetic stirring and then, the solution was heated up to 170 °C. We added 0.5 g of AgCl to the EG solvent to produce the seed, PVP as the capping agent, and EG as the solvent and reducing agent. The products were effectively purified by a precipitation method using acetone solvent as referring to a previous literature.[42] These purified Ag NWs were preserved in ethanol. The concentration of Ag NW solution (119 mg/kg) was analyzed by an inductively coupled plasma-optical emission spectrometer. PAA solution, which is a precursor to CPI, was synthesized by dissolving 1.018 of 6-FDA and 0.569 g of APS in 3.7 g of DMAc solvent under 500 rpm stirring for 5 h.

4.3. Fabrication on Solution-Based Ag NW Temperature Sensors. Flexible Ag NWs patterned (p-Ag NWs) in a CPI film are fabricated by a mold manufactured by a 3D printer and a vacuum filter method. The 3D-printed mold for patterning of an electrode was fabricated using Makerbot Replicator 2X (Makerbot, Boston MA, USA). The mold was self-drawn using 3ds max software and an electrode with a line width of 2 mm was printed using the acrylonitrile-butadiene-styrene filament. A nylon filter paper was sandwiched between a vacuum filtration equipment and the 3D-printed mold. Then, the Ag NW solution was depressurized to obtain an Ag NW electrode patterned on a nylon paper. The p-Ag NWs attached on a nylon membrane was transferred to a glass substrate by a uniaxial pressing machine with a pressure of 3 psi. Then, the PAA solution was coated on the p-Ag NWs on the glass substrate with a doctor blade with a thickness of 50 μm. For the imidization of PAA, thermal heat treatment was conducted at 100, 200, and 230 °C for 0.5, 0.5, and 1 h, respectively, sequentially in a box furnace. Finally, the p-Ag NWs embedded in the CPI film (p-Ag NWs/CPI) naturally detached from a glass substrate in distilled water. The p-Ag NWs/CPI film thickness was measured using a digital micrometer.

4.4. Real-Time Temperature Sensing Using p-Ag NWs/CPI. A total of 80 mL of blood extracted from the Sprague Dawley rats was placed in an EDTA-coated bottle to prevent blood coagulation and was stored in a refrigerator (1−6 °C). The blood was then divided into Falcon tubes into 20 mL aliquots and wrapped with the proposed flexible temperature sensor to observe the individual thermal response. A gold-patterned thin film was used as a connecting wire between the sensor and the PCB to allow the temperature sensor to easily mount on the blood bottle. In addition, a polyethylene-terephthalate film was attached to the front side of the sensor to enhance the mechanical coupling around the ACF bonding. After that, the temperature sensor was mounted on the blood tube and kept in a customized blood box, maintaining a low temperature (1−6 °C) to observe the electrical characteristics concerning temperature. The sequential data acquisition process for temperature monitoring occurs in the following calibration flow; (1) the Ag NW temperature sensor was implemented on the custom built PCB as the abovementioned ACF bonding process. (2) A commercially available Arduino controller has been selected to generate the digitized temperature data. (3) A Wheatstone bridge-type resistor network with the Ag NW temperature sensor has been formed to generate the noise-free differential voltage signals. (4) The bridge network generated differential voltage signals which have been amplified and digitized using a commercially available Arduino-Uno controller for deteriorating the stable and accurate temperature signals. (5) To calibrate the Ag NW temperature sensor, an Arduino controller has been programmed in a way to select the temperature value at a time by manipulating the temperature variations using the combinational procedure of the hot chunk controller (HCC) and Keithley-4200s machines. (6) The Ag NW temperature sensor has been kept in the vacuum chamber to obtain the accurate temperature environment and the Ag NW differential voltage signals have been calibrated simultaneously to optimize the accurate correlation according to the temperature variations. (7) To optimize the wireless communication temperature data, a commercially available bluetooth (BLE) module (HC-06) has been chosen for visualizing the temperature data on the custom-built android application on the mobile phone. (8) Along with the BLE module, a commercially available micro SD card and its adapter module has been adopted to store the data obtained from the Ag NW temperature sensor for a long term. (9) And to compare the Ag NW temperature sensor response, the commercial temperature sensor (SHT21) has been purchased from Sensirion and the circuit layout is shown in the Supporting Information (Figure S7).

4.5. Characterization. The Ag NW and Ag NW-based electrodes were characterized by using field emission scanning electron microscopy (Field Emission SEM, SU5000), high-resolution TEM (Tecnai 200 kV), and atomic force microscopy (XE-100, Park systems). The sheet resistance was measured using a 4-point probe method. Resistance measurements across various temperatures were conducted using a Keithley 4200s instrument, and the temperature was regulated by a HCC.

■ ASSOCIATED CONTENT

Supporting Information

The Supporting Information is available free of charge on the ACS Publications website at DOI: 10.1021/acsami.8b11928.

Additional SEM, optical, AFM images, and a schematic layout of a temperature sensor (PDF)

A video showing experimental results of real-time temperature sensing of p-Ag NWs/CPI (AVI)

■ AUTHOR INFORMATION

Corresponding Authors

*E-mail: idkim@kaist.ac.kr (I.-D.K.).
*E-mail: seonkuk@skku.edu (S.K.).

ORCID

Il-Doo Kim: 0000-0002-9970-2218

Author Contributions

¶D.-Y.Y., U.J., M.N. and S.-J.C. contributed equally.

Notes

The authors declare no competing financial interest.

■ ACKNOWLEDGMENTS

This work was supported by the National Research Foundation of Korea (NRF), grant no. 2014R1A4A1003712 (BRL Program), and Wearable Platform Materials Technology Center (WMC) funded by the National Research Foundation of Korea (NRF) Grant of the Korean Government (MSIP) (no. 2016R1A5A1009926). This work was supported by the

DOI: 10.1021/acsami.8b11928
ACS Appl. Mater. Interfaces 2018, 10, 44678−44685

National Research Foundation of Korea (2015R1A5A1037548 and 2014M3A9D7070732).

REFERENCES

(1) Yao, S.; Swetha, P.; Zhu, Y. Nanomaterial-Enabled Wearable Sensors for Healthcare. *Adv. Healthcare Mater.* **2017**, *7*, 1700889.

(2) Trung, T. Q.; Lee, N.-E. Flexible and Stretchable Physical Sensor Integrated Platforms for Wearable Human-Activity Monitoring and Personal Healthcare. *Adv. Mater.* **2016**, *28*, 4338−4372.

(3) Choi, S.-J.; Kim, S.-J.; Kim, I.-D. Ultrafast Optical Reduction of Graphene Oxide Sheets on Colorless Polyimide Film for Wearable Chemical Sensors. *NPG Asia Mater.* **2016**, *8*, No. e315.

(4) Kim, S.-J.; Choi, S.-J.; Jang, J.-S.; Cho, H.-J.; Kim, I.-D. Innovative Nanosensor for Disease Diagnosis. *Acc. Chem. Res.* **2017**, *50*, 1587−1596.

(5) He, X.; Zi, Y.; Guo, H.; Zheng, H.; Xi, Y.; Wu, C.; Wang, J.; Zhang, W.; Lu, C.; Wang, Z. L. A Highly Stretchable Fiber-Based Triboelectric Nanogenerator for Self-Powered Wearable Electronics. *Adv. Funct. Mater.* **2016**, *27*, 1604378.

(6) Wu, F.; Rüdiger, C.; Yuce, M. Real-Time Performance of a Self-Powered Environmental IoT Sensor Network System. *Sensors* **2017**, *17*, 282.

(7) Gubbi, J.; Buyya, R.; Marusic, S.; Palaniswami, M. Internet of Things (IoT): A Vision, Architectural Elements, and Future Directions. *Future Generat. Comput. Syst.* **2013**, *29*, 1645−1660.

(8) Gutierrez, G.; Reines, H. D.; Wulf-Gutierrez, M. E. Clinical Review: Hemorrhagic Shock. *Crit. Care* **2004**, *8*, 373−381.

(9) Hess, J. R. Red Cell Changes during Storage. *Transfus. Apher. Sci.* **2010**, *43*, 51−59.

(10) Hess, J. R. Measures of Stored Red Blood Cell Quality. *Vox Sang.* **2014**, *107*, 1−9.

(11) Sigle, J. P.; Holbro, A.; Lehmann, T.; Infanti, L.; Gerull, S.; Stern, M.; Tichelli, A.; Passweg, J.; Buser, A. Temperature-Sensitive Indicators for Monitoring RBC Concentrates Out of Controlled Temperature Storage. *Am. J. Clin. Pathol.* **2015**, *144*, 145−150.

(12) DeChristopher, P. J.; Sosler, S. D. Discoveries, and Developments Transforming Blood Banking and Transfusion Medicine—Part 2. *Lab. Med.* **1995**, *26*, 315−321.

(13) Sosler, M.; DeChristopher, P. J. Discoveries and Developments Transforming Blood Banking and Transfusion Medicine—Part 1. *Lab. Med.* **1995**, *26*, 315−321.

(14) Sparrow, R. L. Red Blood Cell Storage and Transfusion-Related Immunomodulation. *Blood Transfus.* **2010**, *8*, s26−s30, DOI: 10.2450/2010.005S.

(15) Palacio, M. G.; Palacio, L. G.; Montealegre, J. J. Q.; Pabón, H. J. O.; del Risco, M. A. L.; Roldán, D.; Salgarriaga, S.; Vásquez, P.; Hernández, S.; Martínez, C. In a Novel Ubiquitous System to Monitor Medicinal Cold Chains in Transportation, Information Systems and Technologies (CISTI). *2017 12th Iberian Conference on, IEEE*, 2017; pp 1−6.

(16) Park, S.-C.; Biswas, S.; Fang, J.; Mozafari, M.; Stauden, T.; Jacobs, H. O. Millimeter Thin and Rubber-Like Solid-State Lighting Modules Fabricated Using Roll-to-Roll Fluidic Self-Assembly and Lamination. *Adv. Mater.* **2015**, *27*, 3661−3668.

(17) Dankoco, M. D.; Tesfay, G. Y.; Benevent, E.; Bendahan, M. Temperature Sensor Realized by Inkjet Printing Process on Flexible Substrate. *Mater. Sci. Eng., B* **2016**, *205*, 1−5.

(18) Chen, Y.; Lu, B.; Chen, Y.; Feng, X. Breathable and Stretchable Temperature Sensors Inspired by Skin. *Sci. Rep.* **2015**, *5*, 11505.

(19) Yan, C.; Wang, J.; Lee, P. S. Stretchable Graphene Thermistor with Tunable Thermal Index. *ACS Nano* **2015**, *9*, 2130−2137.

(20) Trung, T. Q.; Ramasundaram, S.; Hwang, B.-U.; Lee, N.-E. An All-Elastomeric Transparent and Stretchable Temperature Sensor for Body-Attachable Wearable Electronics. *Adv. Mater.* **2015**, *28*, 502−509.

(21) Sibinski, M.; Jakubowska, M.; Sloma, M. Flexible Temperature Sensors on Fibers. *Sensors* **2010**, *10*, 7934−7946.

(22) Chen, K.; Gao, W.; Emaminejad, S.; Kiriya, D.; Ota, H.; Nyein, H. Y. Y.; Takei, K.; Javey, A. Printed Carbon Nanotube Electronics and Sensor Systems. *Adv. Mater.* **2016**, *28*, 4397−4414.

(23) Yang, J.; Wei, D.; Tang, L.; Song, X.; Luo, W.; Chu, J.; Gao, T.; Shi, H.; Du, C. Wearable Temperature Sensor Based on Graphene Nanowalls. *RSC Adv.* **2015**, *5*, 25609−25615.

(24) Hong, S. Y.; Lee, Y. H.; Park, H.; Jin, S. W.; Jeong, Y. R.; Yun, J.; You, I.; Zi, G.; Ha, J. S. Stretchable Active Matrix Temperature Sensor Array of Polyaniline Nanofibers for Electronic Skin. *Adv. Mater.* **2015**, *28*, 930−935.

(25) Kojda, D.; Mitdank, R.; Handwerg, M.; Mogilatenko, A.; Albrecht, M.; Wang, Z.; Ruhhammer, J.; Kroener, M.; Woias, P.; Fischer, S. F. Temperature-Dependent Thermoelectric Properties of Individual Silver Nanowires. *Phys. Rev. B: Condens. Matter Mater. Phys.* **2015**, *91*, 024302.

(26) Cheng, Z.; Liu, L.; Xu, S.; Lu, M.; Wang, X. Temperature Dependence of Electrical and Thermal Conduction in Single Silver Nanowire. *Sci. Rep.* **2015**, *5*, 10718.

(27) Deignan, G.; Goldthorpe, I. A. The Dependence of Silver Nanowire Stability on Network Composition and Processing Parameters. *RSC Adv.* **2017**, *7*, 35590−35597.

(28) Xu, F.; Zhu, Y. Highly Conductive and Stretchable Silver Nanowire Conductors. *Adv. Mater.* **2012**, *24*, 5117−5122.

(29) Lee, D.; Youn, D.-Y.; Luo, Z.; Kim, I.-D. Highly Flexible Transparent Electrodes Using a Silver Nanowires-Embedded Colorless Polyimide Film via Chemical Modification. *RSC Adv.* **2016**, *6*, 30331−30336.

(30) Kim, Y.; Ryu, T. I.; Ok, K.-H.; Kwak, M.-G.; Park, S.; Park, N.-G.; Han, C. J.; Kim, B. S.; Ko, M. J.; Son, H. J.; Kim, J.-W. Inverted Layer-By-Layer Fabrication of an Ultraflexible and Transparent Ag Nanowire/Conductive Polymer Composite Electrode for Use in High-Performance Organic Solar Cells. *Adv. Funct. Mater.* **2015**, *25*, 4580−4589.

(31) Nam, S.; Song, M.; Kim, D.-H.; Cho, B.; Lee, H. M.; Kwon, J.-D.; Park, S.-G.; Nam, K.-S.; Jeong, Y.; Kwon, S.-H.; Park, Y. C.; Jin, S.-H.; Kang, J.-W.; Jo, S.; Kim, C. S. Ultrasmooth, Extremely Deformable and Shape Recoverable Ag Nanowire Embedded Transparent Electrode. *Sci. Rep.* **2014**, *4*, 4788.

(32) Im, H.-G.; Jung, S.-H.; Jin, J.; Lee, D.; Lee, J.; Lee, D.; Lee, J.-Y.; Kim, I.-D.; Bae, B.-S. Flexible Transparent Conducting Hybrid Film Using a Surface-Embedded Copper Nanowire Network: A Highly Oxidation-Resistant Copper Nanowire Electrode for Flexible Optoelectronics. *ACS Nano* **2014**, *8*, 10973−10979.

(33) Choi, S.-J.; Kim, S.-J.; Jang, J.-S.; Lee, J.-H.; Kim, I.-D. Silver Nanowire Embedded Colorless Polyimide Heater for Wearable Chemical Sensors: Improved Reversible Reaction Kinetics of Optically Reduced Graphene Oxide. *Small* **2016**, *12*, 5826−5835.

(34) Choi, S.-J.; Jang, J.-S.; Park, H. J.; Kim, I.-D. Optically Sintered 2D RuO2 Nanosheets: Temperature-Controlled NO2 Reaction. *Adv. Funct. Mater.* **2017**, *27*, 1606026.

(35) Qin, Q.; Yin, S.; Cheng, G.; Li, X.; Chang, T.-H.; Richter, G.; Zhu, Y.; Gao, H. Recoverable Plasticity in Penta-Twinned Metallic Nanowires Governed by Dislocation Nucleation and Retraction. *Nat. Commun.* **2015**, *6*, 5983.

(36) Chen, H.; Gao, Y.; Zhang, H.; Liu, L.; Yu, H.; Tian, H.; Xie, S.; Li, J. Transmission-Electron-Microscopy Study on Fivefold Twinned Silver Nanorods. *J. Phys. Chem. B* **2004**, *108*, 12038−12043.

(37) Min, U.; Chang, J.-H. Colorless and Transparent Polyimide Nanocomposite Films Containing Organoclay. *J. Nanosci. Nanotechnol.* **2011**, *11*, 6404−6409.

(38) Li, C. C.; Drymiotis, F.; Liao, L. L.; Dai, M. J.; Liu, C. K.; Chen, C. L.; Chen, Y. Y.; Kao, C. R.; Snyder, G. J. Silver as A Highly Effective Bonding Layer for Lead Telluride Thermoelectric Modules Assembled by Rapid Hot-Pressing. *Energy Convers. Manage.* **2015**, *98*, 134−137.

(39) Yang, S.-B.; Choi, H.; Lee, D. S.; Choi, C.-G.; Choi, S.-Y.; Kim, I.-D. Improved Optical Sintering Efficiency at the Contacts of Silver Nanowires Encapsulated by a Graphene Layer. *Small* **2014**, *11*, 1293−1300.

DOI: 10.1021/acsami.8b11928
ACS Appl. Mater. Interfaces 2018, 10, 44678−44685

(40) Kim, S.; Kwon, H.-J.; Lee, S.; Shim, H.; Chun, Y.; Choi, W.; Kwack, J.; Han, D.; Song, M.; Kim, S.; Mohammadi, S.; Kee, I.; Lee, S. Y. Low-Power Flexible Organic Light-Emitting Diode Display Device. *Adv. Mater.* **2011**, *23*, 3511−3516.
(41) Kwon, H.; Choi, W.; Lee, D.; Lee, Y.; Kwon, J.; Yoo, B.; Grigoropoulos, C. P.; Kim, S. Selective and Localized Laser Annealing Effect for High-Performance Flexible Multilayer MoS2 Thin-Film Transistors. *Nano Res.* **2014**, *7*, 1137−1145.
(42) Li, B.; Ye, S.; Stewart, I. E.; Alvarez, S.; Wiley, B. J. Synthesis and Purification of Silver Nanowires To Make Conducting Films with a Transmittance of 99%. *Nano Lett* **2015**, *15*, 6722−6726.

DOI: 10.1021/acsami.8b11928
ACS Appl. Mater. Interfaces 2018, 10, 44678−44685